Turkish Journal of Science & Technology
17(1), 55-64, 2022

Research Paper
https://doi.org/10.55525/tjst.1057940

Investigation of an Outer Rotor In-Wheel Switched Reluctance Motor for Electric Vehicles by Finite Element Method

Zeki OMAÇ[1*]
[1] Department of Electrical and Electronics Engineering, Faculty of Engineering, Munzur University, Tunceli, Turkey
[*1] zomac@munzur.edu.tr

(Geliş/Received: 14/01/2022; Kabul/Accepted: 22/02/2022)

Abstract: The demand of fossil fuel vehicles has decreased due to carbon emissions. Recently, electric vehicles (EV) with electric motor propulsion have got attention due to their zero carbon emissions and high efficiency. In this study, an outer rotor in-wheel switched reluctance motor (IWSRM) with 18 poles on the stator and 24 poles on the rotor, designed for the propulsion of electric vehicles, is investigated in two-dimensional Finite Element Method (FEM). The magnetic field distributions of IWSRM for different rotor positions at nominal current are obtained. Then, the torque and phase inductance are calculated. As a result, the designed outer rotor IWSRM provided low torque ripple.

Key words: In-Wheel Switched Reluctance Motor, Finite Element Method, Electric Vehicle.

Elektrikli Araçlar için Rotoru Dışta Tekerlek İçi bir Anahtarlamalı Relüktans Motorun Sonlu Elemanlar Yönteminde İncelenmesi

Öz: Karbon salınımları nedeniyle fosil yakıtlı araçlara ilgi azalmaktadır. Sıfır karbon salınımları ve yüksek verimleri nedeniyle son zamanlarda elektrik motoru tahrikli araçlar gündeme gelmiştir. Bu çalışmada, elektrikli araçların tahriki için tasarlanmış, statorunda 18 kutup ve rotorunda 24 kutup olan rotoru dışta tekerlek içi bir anahtarlamalı relüktans motor (TARM), iki boyutlu Sonlu Elemanlar Yönteminde (SEY) incelenmiştir. Nominal akımda farklı rotor konumları için TARM'ın alan dağılımları elde edilmiş, ürettiği nominal moment hesaplanmış ve endüktans eğrisi çıkarılmıştır. SEY analiz sonucunda, incelenen TARM'de düşük moment dalgalanması elde edilmiştir.

Anahtar kelimeler: Tekerlek İçi Anahtarlamalı Relüktans Motor, Sonlu Elemanlar Yöntemi, Elektrikli Araç.

1. Introduction

Recently, interest regarding electric vehicles has raised because of their higher efficiency, zero carbon emission, noiseless operation and low cost compared to internal combustion engines [1-2]. In addition, electric vehicles with in-wheel electric motors do not need gears and transmission parts, which gives these vehicles an additional advantage.

In electric vehicles, permanent magnet synchronous motor (PMSM), induction motor (IM) and switched reluctance motor (SRM) are used as propulsion motors [3-4]. These motors have some advantages and disadvantages in terms of cost, losses, and efficiency. Although the PMSM is a highly efficient motor, it is the most expensive electric motor due to the magnets used in its rotor. However, these magnets are not used in the IM and SRM, so the cost of the IM and SRM are lower than PMSM. Compared to SRM, which does not have winding on the rotor, the losses in IM are high due to the conductors in the rotor. Therefore, SRM is a motor with the lowest cost with its simple and rugged motor structure, invulnerability to harsh operating conditions, robust rotor, low maintenance cost and decreased losses. In addition, SRMs have salient pole structure in stator and rotor facilitating the cooling of the heat generated due to losses [5-12].

To generate larger torque values, the SRM is operated at high magnetic saturation. Therefore, the nonlinear magnetization curve of the iron sheet used in the stator and rotor should be considered when the magnetic field distribution of the SRM is obtained. It is easier to assemble the outer rotor in-wheel switched reluctance motor (IWSRM) to the wheel rim, and then the torque produced is greater than the conventional SRM [6]. For solving these magnetic problems, FEM, a computer-aided numerical method, is a suitable method.

In the SRM for a continuous rotational motion, the current flows through the phases sequentially. In other words, the torque produced by the SRM is equal to the sum of the torques sequentially produced by the phases. The torque produced by a phase at constant current is a curve varying from zero to maximum depending on the

* Corresponding author: zomac@munzur.edu.tr. ORCID Number of authors: [1] 0000-0002-9339-8243

position. This causes a ripple in the total torque produced. The torque ripple causes acoustic noises in SRM [13-18].

In the literature, different IWSRM models designed for electric vehicles have been emphasized. In [2], a IWSRM model with double teeth per pole on a 6/16 pole stator is examined. In [5], the design of an 18/12 pole IWSRM is best done using a Pareto-based multi-objective differential evolution algorithm. In [7], a new 18/12 pole IWSRM for electric vehicle is designed, FEM analysis and control are performed. In [9], an 8/6 pole IWSRM is designed using multi-objective optimization.

In this study, the magnetic field distribution, torque, and inductance variations of outer rotor IWSRM are calculated from two-dimensional FEM for electric vehicles.

2. Outer Rotor in Wheel Switched Reluctance Motor

Unlike the conventional SRM motor structure, the rotor is outside, and the stator is inside in an outer rotor in wheel SRM. The cross-sectional view of the 18/24-pole IWSRM is shown in Figure 1. In addition, stator and rotor outer diameters and other pole length dimensions are shown in Figure 2. Furthermore, all other motor dimensions are given in Table 1.

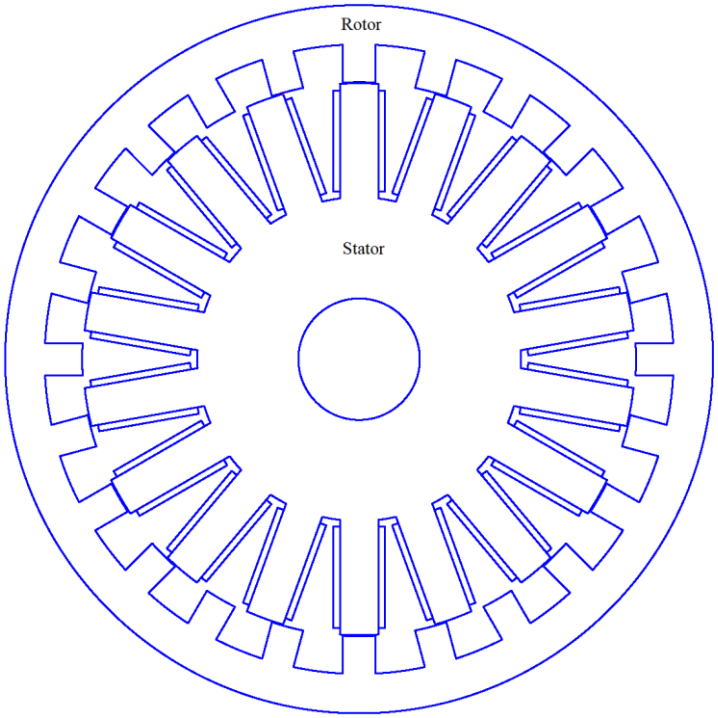

Figure 1. The cross-sectional view of outer rotor IWSRM.

For constant current, the torque produced in one phase of the SRM can be calculated from the equation (1) [12].

$$T_e = \frac{\partial W_m}{\partial \theta} \tag{1}$$

Where, T_e, W_m and θ denote electromagnetic torque, co-energy, and rotor position, respectively. The total torque produced in SRM is equal to the sum of the torques produced by the individual phases. The total torque for a three-phase SRM can be written as in equation (2).

$$T_t = T_a(\theta, i_a) + T_b(\theta, i_b) + T_c(\theta, i_c) \tag{2}$$

Here, T_t the total torque, T_a, T_b and T_c represent the torque produced in phases a, b, and c, respectively.

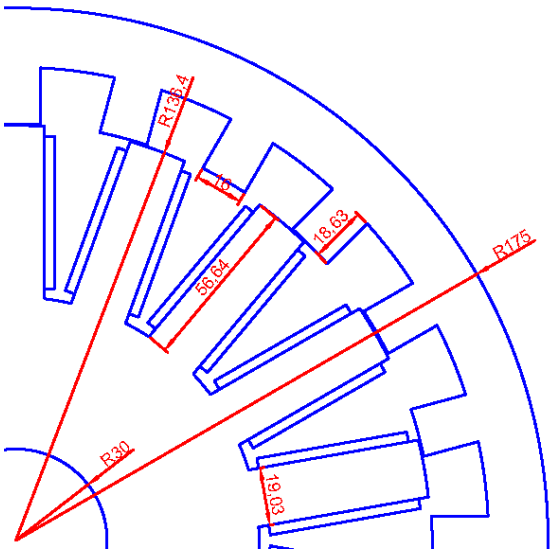

Figure 2. The representation of some dimensions of IWSRM on a quarter view.

Table 1. Parameters of outer rotor in-wheel switched reluctance motor.

Parameter	Value
Number of stator poles (N_s)	18
Number of rotor poles (N_r)	24
Rotor outer diameter (mm)	350
Stator outer diameter (mm)	273.8
Package length (mm)	55
Air gap (mm)	0.5
Shaft diameter (mm)	60
Stator pole arc (degree)	8
Rotor pole arc (degree)	7
Stator pole width (mm)	19.03
Rotor pole width (mm)	16
Stator pole height (mm)	56.64
Rotor pole height (mm)	18.63

3. Finite Element Method Analysis of Outer Rotor IWSRM and Results

In the Finite Element Method, the geometry of outer rotor IWSRM, stator, rotor and air gap are divided into small triangular elements, as shown in Figure 3 [17]. To minimize the amount of error and to calculate accurate results, the air gap region between the stator and the rotor, where there is a large change in magnetic parameters, is divided into smaller triangular elements in as four layers as shown in Figure 4. The air region outside the IWSRM is meshed with larger triangular elements. A zero-vector potential is defined at the boundary of the region of solution. A current density of J=21161876 A/m^2 is applied to the windings on six poles forming a phase for a nominal current of 75 A. Steel 1008 sheet is chosen for the stator and rotor iron sheets.

The rotor position is rotated one degree from the aligned to the unaligned position, and the magnetic field distribution for the IWSRM is obtained for each rotor position, and the produced torque and phase inductance are calculated for a single phase. The air gap magnetic field distribution is given in Figure 5 for the rotor position θ=5°. The magnetic field distributions obtained from the two-dimensional FEM are shown in Figure 6 (a) and (b) for rotor positions θ=0° and θ=5°, respectively. The graph of the torque produced in one phase depending on the rotor position at the nominal current is shown in Figure 7 and the graph of inductance is shown in Figure 8.

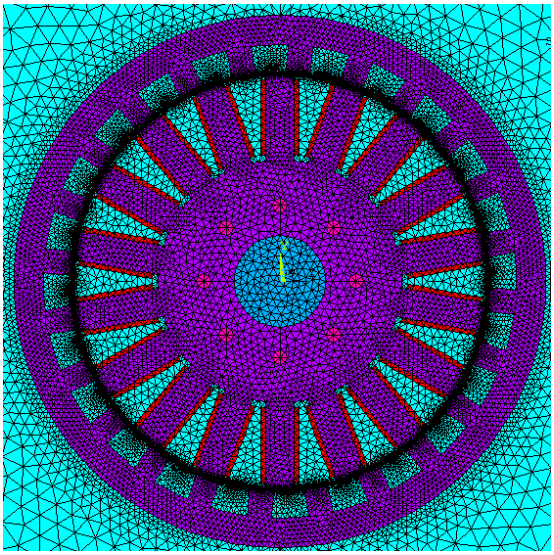

Figure 3. The meshed of outer rotor IWSRM.

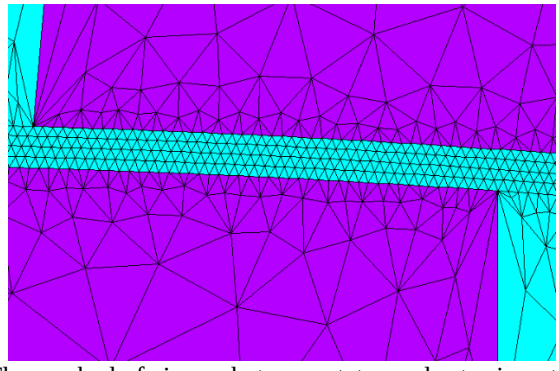

Figure 4. The meshed of air gap between stator and rotor in outer rotor IWSRM.

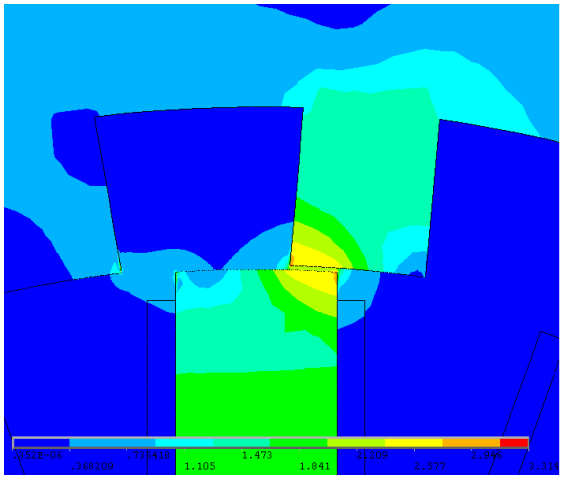

Figure 5. The magnetic field distribution in air gap region for θ=5° rotor position.

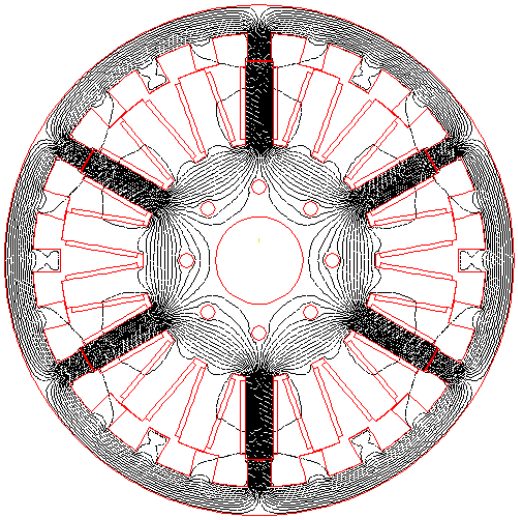

(a)

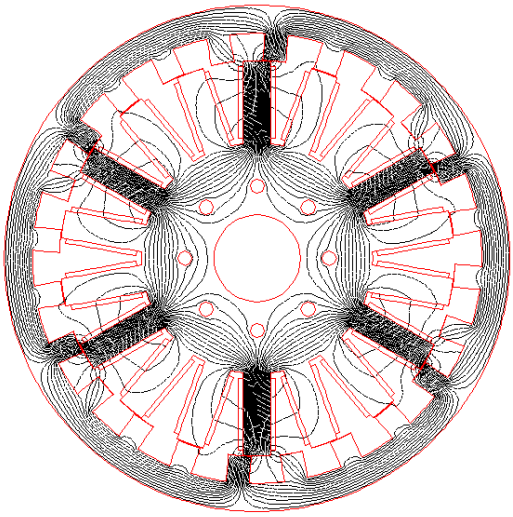

(b)

Figure 6. Magnetic field distributions for different rotor positions (a) θ=0°, (b) θ=5°.

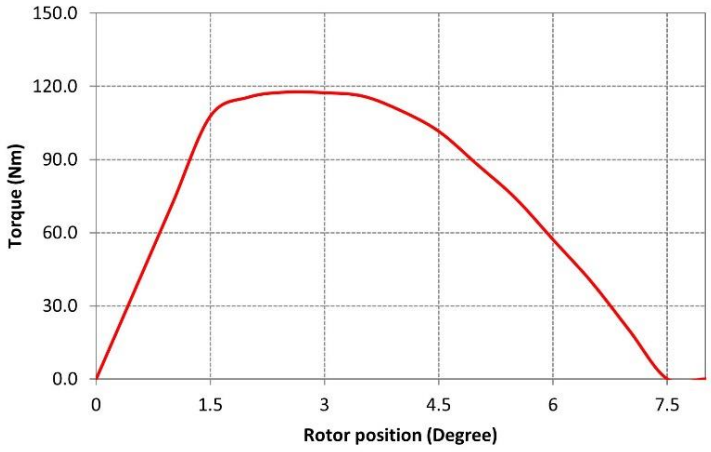

Figure 7. The graph of the torque generated by a phase at the nominal current depending on the rotor position.

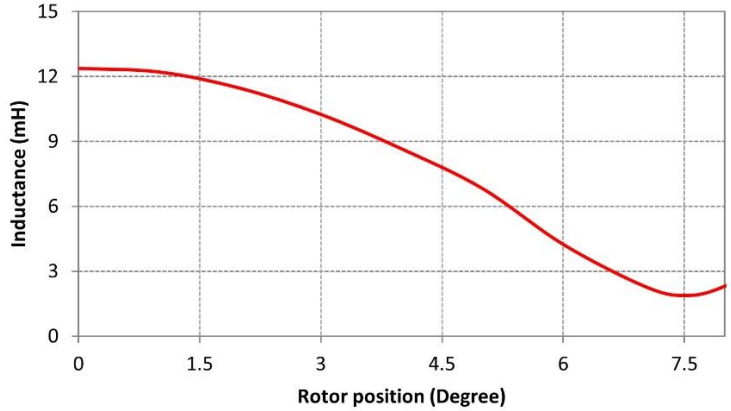

Figure 8. The graph of a phase inductance with respect to the rotor position.

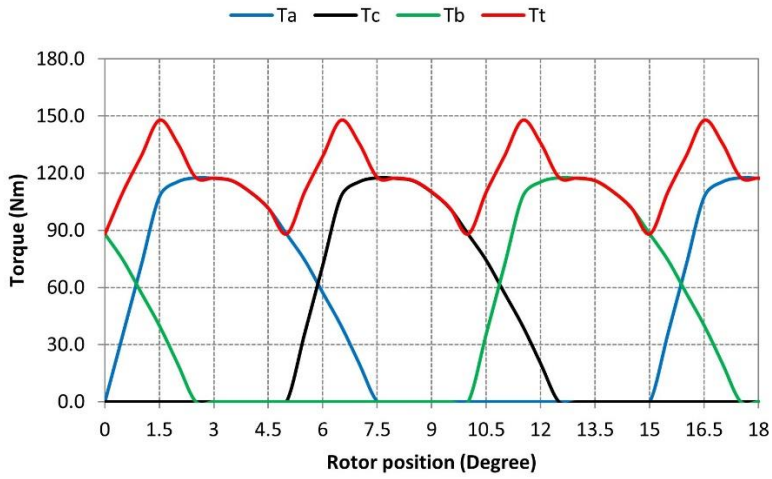

Figure 9. The graph of phase torques and total torque with respect to the rotor position at the nominal current.

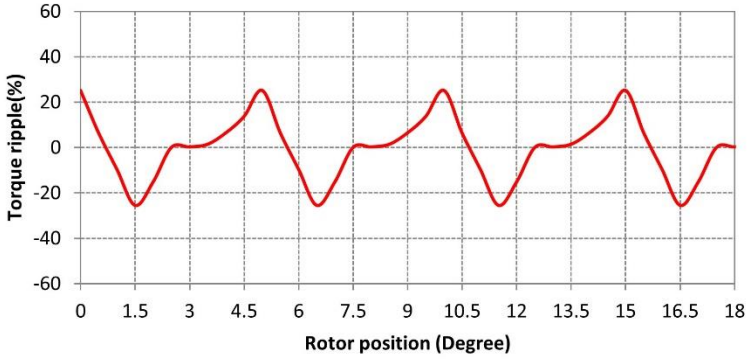

Figure 10. The graph of torque ripple with respect to the rotor position at the nominal current.

In outer rotor IWSRM, the torques separately produced by phases a, b and c depending on the rotor position at the nominal current, and the total torque produced are displayed in Figure 9. In addition, the percentage ripple in the total torque is given in figure 10.

In designing of outer rotor IWSRM models, the low torque ripple is desired for smooth speed response. For example, in the SRM model with 18 poles on the stator and 12 poles on the rotor, designed for hybrid electric vehicles in a study [10], the torque ripple varies between ±36% for square wave current. In this study, the investigated the outer rotor IWSRM model with the 18/24 poles, the torque ripple is ±25% for square wave current. Therefore, the investigated the outer rotor IWSRM model has ±11% lower torque ripple than the 18/12 pole SRM model in [10]. Radial forces cause acoustic noises in the outer rotor IWSRM. Another source of acoustic noise is torque ripple. When torque ripple is reduced, the acoustic noise will be lower at the same rate due to the torque ripple.

4. Mathematical Model of Outer Rotor IWSRM and Simulation Results

If the mutual inductance between phases is neglected, the voltage can be written for a phase of the outer rotor IWSRM in equation (3) [12-13].

$$v = iR + \frac{d\psi(\theta, i)}{dt} \tag{3}$$

Where v is the phase voltage, R is the phase resistance, i is the phase current, ψ is the magnetic flux and θ is the rotor position. If the relation $\psi = iL$ is used for the magnetic flux, the voltage of a phase becomes as equation (4).

$$v = iR + L(\theta, i)\frac{di}{dt} + i\omega_m \frac{dL(\theta, i)}{d\theta} \tag{4}$$

Where ω_m is the rotor angular velocity and L is the phase inductance. The torque induced in the rotor can be calculated from equation (5).

$$T_e = \frac{1}{2} i^2 \frac{dL(\theta, i)}{d\theta} \tag{5}$$

Where T_e is the torque induced in the rotor. The mechanical motion equation of the outer rotor IWSRM is given in equation (6).

$$T_e = J\frac{d\omega_m}{d\theta} + B\omega_m + T_L \tag{6}$$

Where, J is the moment of inertia, B is the friction coefficient and T_L is the load torque.

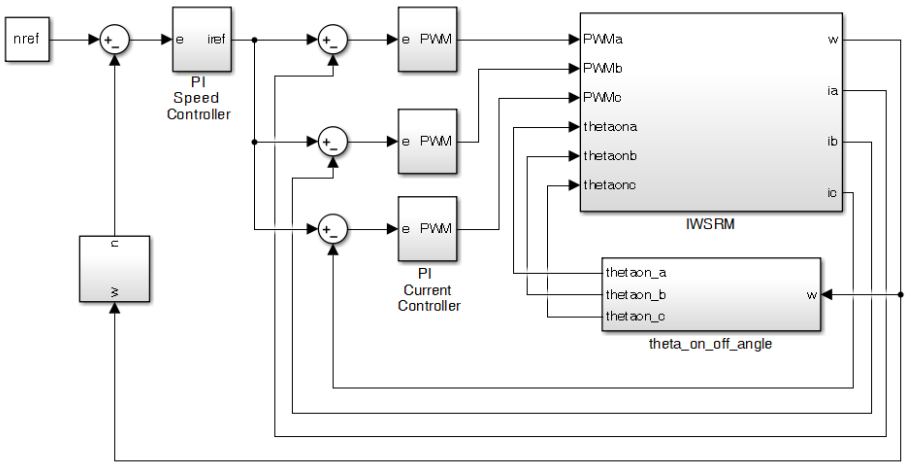

Figure 11. Matlab/Simulink model of the outer rotor IWSRM.

The dynamic model of the outer rotor IWSRM prepared in Matlab Simulink software is shown in Figure 11. The simulation model parameters and values of the outer rotor IWSRM are given in Table 2. The simulation results of the outer rotor IWSRM are given in Figure 12 for speed, torque, and phase currents under T_L=80 Nm load torque at n=200 rpm reference speed. Proportional integral (PI) controller is used for speed and current control of the outer rotor IWSRM. When the speed graph is examined, the outer rotor IWSRM rotor speed reaches the reference speed in a short time and catches the steady state with a small oscillation. When the outer rotor IWSRM is started, the phase currents take large values. After the outer rotor IWSRM is started, phase currents decrease to normal values. Likewise, the torque ripple produced in the rotor during starting is high. When the rotor speed reaches the reference speed, the torque graph becomes smooth.

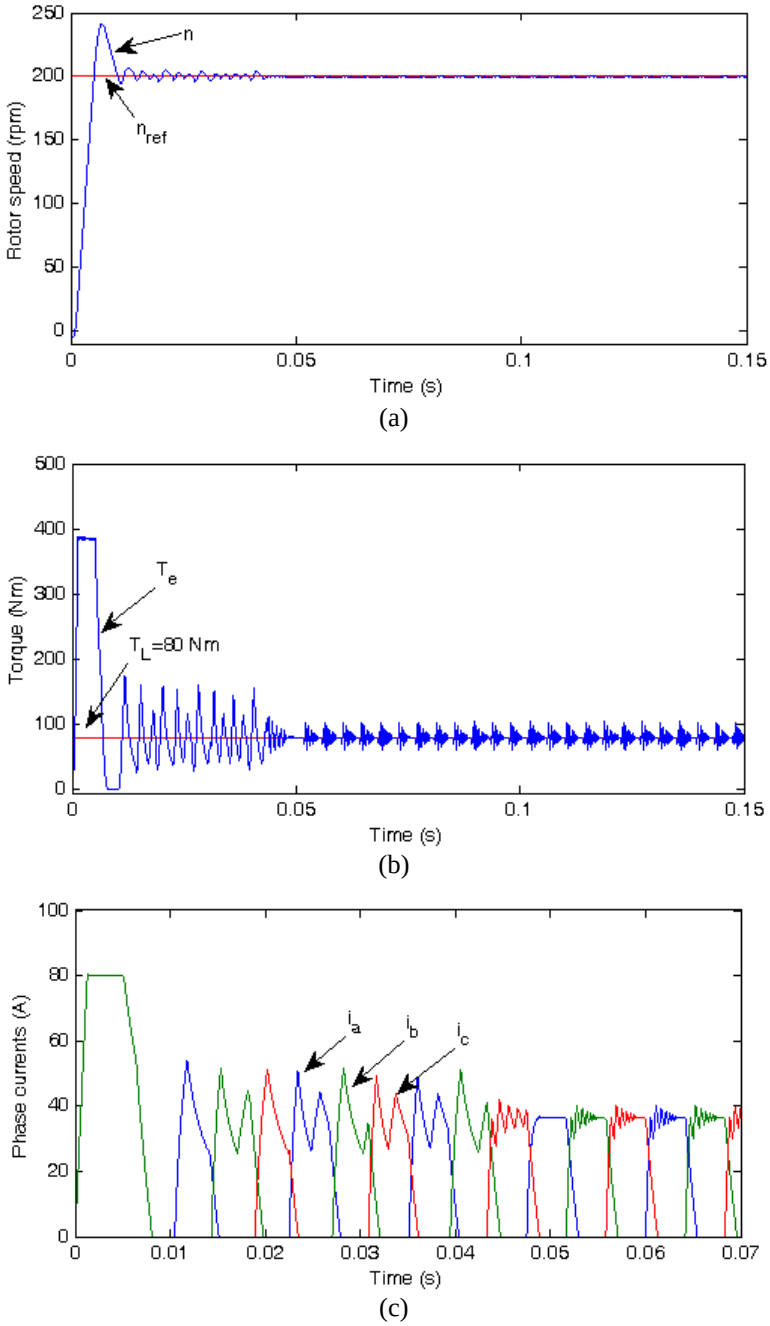

Figure 12. Simulation results for n_{ref}=200 rpm reference speed, and T_L=80 Nm load torque (a) Rotor speed, (b) Torque, (c) Phase currents.

Table 2. Simulation parameters of the outer rotor IWSRM.

Parameter	Value
DC bus voltage	300 V
A phase resistance (R)	0.5 Ω
Friction factor (B)	0.0055 Nm/(rad/s)
Inertia of rotor (J)	0.0593 Kg.m^2
Proportional coefficient (K_p)	30
Integral coefficient (K_i)	0.5
Load torque (T_L)	80 Nm

5. Conclusion

In this study, outer rotor in wheel switched reluctance motor with 18 poles in its stator and 24 poles in its rotor designed for electric vehicles is investigated using FEM under nonlinear magnetic conditions. In outer rotor IWSRM, a phase is formed by simultaneously exciting the windings on six opposite poles in the stator. Thus, the outer rotor IWSRM converter is simpler and produces larger torques by using fewer solid-state switches. At the nominal current, the magnetic field distribution of the outer rotor IWSRM is obtained by rotating the rotor at an angle of each one degree. In addition, a phase inductance, torque, and total torque are calculated at the nominal current. As a result, low torque ripple is obtained in the investigated model of outer rotor IWSRM.

References

[1] Yang Z, Shang F, Brown I P, and Krishnamurthy M. Comparative study of interior permanent magnet, induction, and switched reluctance motor drives for EV and HEV applications. IEEE Trans Transp Electrific 2015; **1(**3): 245-254.

[2] Zhu J, Cheng K W E, Xue X, and Zou Y. Design of a new enhanced torque in-wheel switched reluctance motor with divided teeth for electric vehicles. IEEE Trans Magn 2017; 53(11).

[3] Gong C, Li S, Habetler T, and Zhou P. Acoustic modeling and prediction of ultrahigh-speed switched reluctance machines based on multiphysics finite element analysis. IEEE Trans Ind Appl 2021; 57(1):198- 207.

[4] Chiba A, Kiyota K, Hoshi N, Takemoto M, and Ogasawara S. Development of a rare-earth-free SR motor with high torque density for hybrid vehicles. IEEE Trans Energy Convers 2015; 30(1): 175-182.

[5] Öksüztepe E. In-wheel switched reluctance motor design for electric vehicles by using pareto based multi objective differential evolution algorithm. IEEE Transs Vehic Technol 2017; 66(6): 4706-4715.

[6] Rallabandi V, Han P, Wu J, Cramer A M, Ionel D M, and Zhou P, Design optimization and comparison of direct-drive outer-rotor SRMs based on fast current profile estimation and transient FEA. IEEE Trans Ind Appl 2021; 57(1): 236-245.

[7] Omaç Z, Polat M, Öksüztepe E, Yıldırım M, Yakut O, Eren H, Kaya M, and Kürüm H. Design, analysis, and control of in-wheel switched reluctance motor for electric vehicles. Elec Eng 2018;100: 865–876.

[8] Yildirim M, Polat M, Öksüztepe E, Omaç Z, Yakut O, Eren H, Kaya M, Kürüm H. Designing in-wheel switched reluctance motor for electric vehicles 2014; IEEE PEMC'14: 793-798.

[9] Xue X D, Cheng K W E, Ng T W, and Cheung N C. Multi-objective optimization design of in-wheel switched reluctance motors in electric vehicles. IEEE Trans Ind Electron 2010; **57(**9): 2980-2987.

[10] Furqani J, Wiguna C A, Chiba A, Gundogmus O, Sozer Y, and Purwadi A. Experimental verification of acoustic noise and radial force sum variation in switched reluctance motor. IEEE Trans Ind Appl 2021; **57(**1): 2481- 2493.

[11] Kiyota K, Kakishima T, Chiba A, Rahman M A. Cylindrical rotor design for acoustic noise and windage loss reduction in switched reluctance motor for HEV applications. IEEE Trans Ind Appl 2016; **52(**1): 154-162.

[12] Desai P C, Krishnamurthy M, Schofield N, Emadi A. Novel switched reluctance machine configuration with higher number of rotor poles than stator poles: concept to implementation. IEEE Trans Ind Electron 2010; **57(**2): 649-659.

[13] Omaç Z. Fuzzy-logic-based robust speed control of switched reluctance motor for low and high speeds. Turk J Elec Eng & Comp Sci 2019; 27(1): 316–329.

[14] Omaç Z, Polat M, Kaya M, Öksüztepe E, Eren H, Yıldırım M, Kürüm H. New trends in electrical vehicle powertrains, Outer rotor srm design for electric vehicle without reducer via speed-up evolutionary algorithm. UK: IntechOpen, 2018. pp.129-151.

[15] Omaç Z, Cevahir C. Control of switched reluctance generator in wind power system application for variable speeds. Ain Shams Eng J 2021; **12**: 2665-2672.

[16] Omaç Z. Design and analysis of a water pumping system with photovoltaic source and switched reluctance motor. Balkan J of Elec & Comp Eng 2019; **7**(3): 355-361.

[17] Omaç Z, Kürüm H, and Selçuk A H. Design, analysis and control of a switched reluctance motor having 18/12 poles. Fırat Uni Sci & Eng J 2007; **3**(19) 339-346.
[18] Omaç Z, Kürüm H, and Selçuk A H. Digital current control of switched reluctance motor. Inter J Elec & Power Eng 2011; 5:54-61.